ARTICLES
PUBLISHED ONLINE: 26 JANUARY 2015 | DOI: 10.1038/NNANO.2014.323
nature nanotechnology

Gate-tunable phase transitions in thin flakes of 1T-TaS_2

Yijun Yu[1,2], Fangyuan Yang[1,2], Xiu Fang Lu[2,3,4], Ya Jun Yan[1,2,3], Yong-Heum Cho[5], Liguo Ma[1,2], Xiaohai Niu[1,2], Sejoong Kim[6], Young-Woo Son[6], Donglai Feng[1,2], Shiyan Li[1,2], Sang-Wook Cheong[5,7], Xian Hui Chen[2,3,4] and Yuanbo Zhang[1,2]*

The ability to tune material properties using gating by electric fields is at the heart of modern electronic technology. It is also a driving force behind recent advances in two-dimensional systems, such as the observation of gate electric-field-induced superconductivity and metal–insulator transitions. Here, we describe an ionic field-effect transistor (termed an iFET), in which gate-controlled Li ion intercalation modulates the material properties of layered crystals of 1T-TaS_2. The strong charge doping induced by the tunable ion intercalation alters the energetics of various charge-ordered states in 1T-TaS_2 and produces a series of phase transitions in thin-flake samples with reduced dimensionality. We find that the charge-density wave states in 1T-TaS_2 collapse in the two-dimensional limit at critical thicknesses. Meanwhile, at low temperatures, the ionic gating induces multiple phase transitions from Mott-insulator to metal in 1T-TaS_2 thin flakes, with five orders of magnitude modulation in resistance, and superconductivity emerges in a textured charge-density wave state induced by ionic gating. Our method of gate-controlled intercalation opens up possibilities in searching for novel states of matter in the extreme charge-carrier-concentration limit.

The competition, coexistence and cooperation of various collectively ordered electronic states in two-dimensional systems has been a breeding ground for novel states of matter[1]. Controllable manipulation of the various phases through gate-tunable charge doping may lead to a new device paradigm for future material science and technology[2–7]. The transition-metal dichalcogenide (TMD) 1T-TaS_2 is a layered two-dimensional atomic crystal known to develop a peculiar Mott phase at low temperatures[8–10]. With a rich set of charge ordered states delicately balanced on a similar energy scale[8,11–13], it provides a unique opportunity for such manipulation[14–17]. However, the large carrier concentration already present in metallic 1T-TaS_2 poses a great challenge. Tipping the balance of various phases in 1T-TaS_2 requires a charge doping level that is comparable to its initial carrier concentration, and thus calls for extreme doping capability well beyond conventional gate electric-field-induced doping levels in semiconductor devices, or even electron-double-layer (EDL) surface gating using ionic liquid[18–20].

We develop a new doping method that utilizes a gate electric field to drive Li ions in and out of the layered 1T-TaS_2 and introduces high doping levels in each atomic layer. This is realized in a device referred to as an ionic field-effect transistor (iFET), which controls the electronic properties of a layered material (1T-TaS_2 in our case) by gate-controlled intercalation (for device structure see Fig. 1b). In this Article we explore previously inaccessible parameter space in 1T-TaS_2-based iFETs following two pathways: (1) reducing the dimensionality of 1T-TaS_2 by thinning it down to a few atomic layers and (2) doping the 1T-TaS_2 by gate-controlled intercalation. Both pathways modify the energetics of the charge-density wave (CDW) phases and dramatically modulate the electronic properties of the 1T-TaS_2. In particular, superconductivity emerges inside a textured CDW phase as a result of gate doping. Our complete phase diagram for the first time investigates the importance of dimensionality and gate-controlled ionic doping in layered atomic crystals, and provides fresh insights into the relations between the superconducting phase and various other charge-ordered phases.

Thickness-dependent CDW phase transitions

We started with 1T-TaS_2 single crystals grown by a standard vapour transport method (Supplementary Section I). The 1T-TaS_2 crystal has a layered structure, in which each atomic layer is composed of a plane of Ta atoms sandwiched by S atoms in an octahedral arrangement[11,13]. Bulk 1T-TaS_2 undergoes a series of CDW transitions as the temperature is lowered. It enters a metallic incommensurate CDW (ICCDW) phase below 550 K, a textured nearly commensurate CDW (NCCDW) phase below 350 K and a commensurate CDW (CCDW) phase below 180 K. The low-temperature CCDW phase is characterized by a $\sqrt{13} \times \sqrt{13}$ superlattice of David-stars formed by twelve Ta atoms clustered around a thirteenth Ta atom[8]. The periodic lattice distortion creates energy gaps in the 1T-TaS_2 bandstructure and leaves exactly one conduction electron per David-star[8]. The on-site Coulomb repulsion further localizes this conduction electron and produces a Mott insulator state that has been confirmed by various experiments[9,10,21]. The neighbouring NCCDW phase consists of trigonally packed CCDW domains separated by metallic regions that are not fully distorted[13,22]. Finally, in the high-temperature ICCDW phase, the

[1]State Key Laboratory of Surface Physics and Department of Physics, Fudan University, Shanghai 200433, China. [2]Collaborative Innovation Center of Advanced Microstructures, 22 Hankou Road, Gulou, Nanjing 210093, China. [3]Hefei National Laboratory for Physical Science at Microscale and Department of Physics, University of Science and Technology of China, Hefei, Anhui 230026, China. [4]Key Laboratory of Strongly Coupled Quantum Matter Physics, University of Science and Technology of China, Hefei, Anhui 230026, China. [5]Laboratory for Pohang Emergent Materials and Department of Physics, Pohang University of Science and Technology, Pohang 790-784, Korea. [6]Korea Institute for Advanced Study, Hoegiro 87, Dongdaemun-gu, Seoul, Korea. [7]Rutgers Center for Emergent Materials and Department of Physics and Astronomy, Rutgers University, Piscataway, New Jersey 08854, USA.
*e-mail: zhyb@fudan.edu.cn

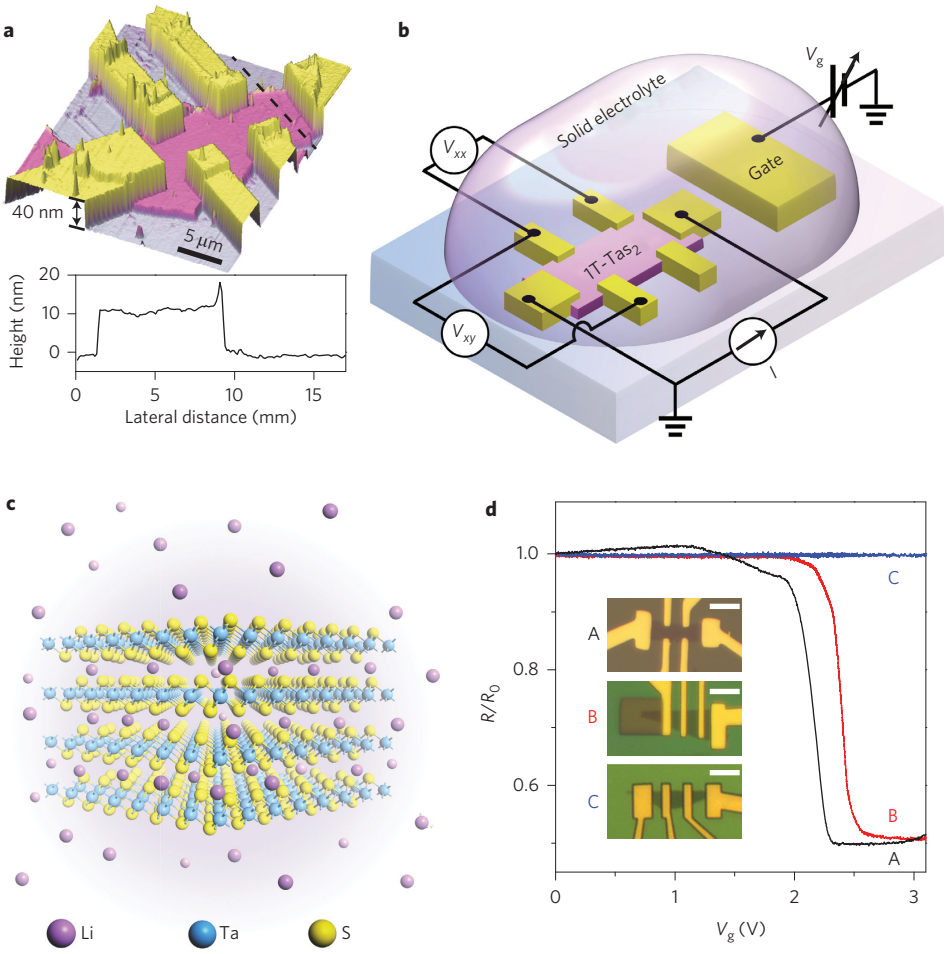

Figure 1 | Gate-controlled intercalation in a 1T-TaS_2-based iFET. a, Top: Three-dimensional rendering of AFM topography of a 1T-TaS_2 thin-flake device. False colours are chosen to match the real colours seen under an optical microscope. Bottom: Cross-sectional profile of the thin flake along the dashed black line. **b**, Schematic structure of 1T-TaS_2 iFET and measurement set-up. **c**, Illustration of Li intercalated into layered 1T-TaS_2. **d**, Resistance R (normalized to its initial value R_0 in the NCCDW phase) of 1T-TaS_2 thin flakes during an up-sweep of V_g at $T = 325$ K. Sample A (black) is fully exposed to solid electrolyte during measurement. The corner of sample B (red) is exposed to solid electrolyte while the active area (the region between the electrodes) is protected by a layer of spin-coated PMMA. Sample C (blue) is fully protected by PMMA. The drop in resistance by one-half in samples A and B is due to the NCCDW/ICCDW phase transition described in the text. Scale bars, 5 μm.

CDW aligns with the 1T-TaS_2 lattice and exhibits normal metallic behaviour[13]. The 1T-TaS_2 thin-flake samples used in this study were cleaved from bulk crystal by mechanical exfoliation, and metal electrodes were then fabricated on top using standard electron-beam lithography (Fig. 1a). The CDW transitions in these devices manifest themselves as sudden jumps in the temperature-dependent sample resistance, as shown in Fig. 2a.

The importance of dimensionality for the CDW phases in 1T-TaS_2 was probed by studying pristine thin flakes with thicknesses varying down to ~2 nm. We discovered that both CCDW/NCCDW and NCCDW/ICCDW phase transitions are strongly modulated by sample thickness (Fig. 2a), an effect that eluded previous attempts[23]. As the sample thickness was reduced, both transitions were shifted to lower temperatures during cooldown (warm-up transitions are discussed in Supplementary Section VII), then suddenly vanished at critical thicknesses of ~10 nm and ~3 nm, respectively. Meanwhile an insulating behaviour prevailed in all samples below 3 nm (Fig. 2b).

The observed critical thicknesses hint at the three-dimensional nature of CDW ordering in 1T-TaS_2. Early studies[12,24–28] have suggested 13-layer (~7.8 nm) and 3-layer (~1.8 nm) periodicities in the out-of-plane direction in the CCDW and NCCDW phases, respectively. (A quasi-ordered stacking in the CCDW phase was also proposed[29,30].) Such periodicities arise as the structure attempts to stabilize the in-plane charge order while minimizing the sum of interlayer Coulomb and tunnelling energy[26]. Our observed critical thicknesses agree reasonably well with the proposed periodicities. We note, however, that the dielectric environment and surface impurities may also play a role in determining the critical thicknesses, because thinner samples are subject to stronger influences from surface effects due to the increased surface-area-to-volume ratio. Our observations expose the fragility of the CDW phases and point to the vital role of dimensionality in sustaining long-range charge ordering in 1T-TaS_2.

Gate-controlled Li ion intercalation in 1T-TaS_2 iFETs

We now turn to study 1T-TaS_2 thin flakes under gate modulation in an iFET configuration. A schematic of the device is presented in Fig. 1b. Gel-like solid electrolyte ($LiClO_4$ dissolved in polyethylene oxide (PEO) matrix, see Methods) was used as the gate medium, covering both the thin flake and the metal side gate. Using an 8-nm-thick flake as an example, the effect of gate bias V_g is shown in Fig. 1d (sample A, black curve). We clearly observe a resistance drop to half of its original value at $V_g \approx 2$ V during the gate sweep, which is identified as a doping-induced NCCDW/ICCDW phase transition (Supplementary Section III). Such a phase

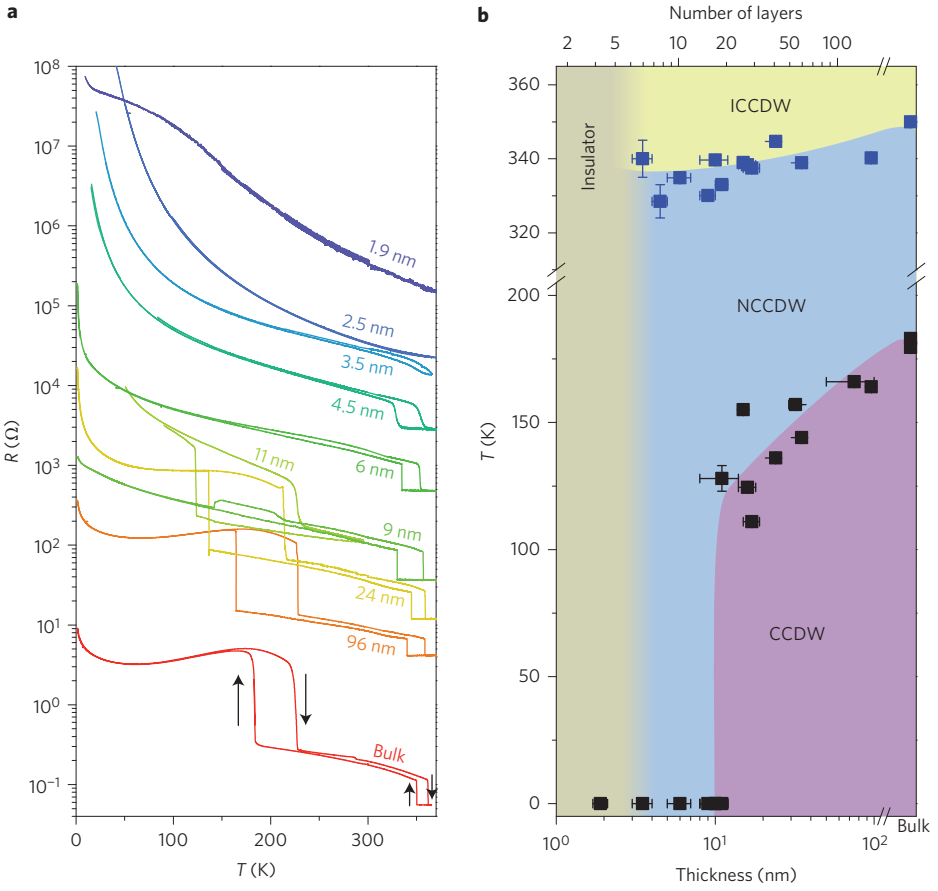

Figure 2 | CDW phases in pristine 1T-TaS_2 thin flakes with varying thicknesses. a, Resistance as a function of temperature for pristine 1T-TaS_2 thin-flake samples with varying thicknesses. Red curve: Typical behaviour of bulk crystal. Arrows indicate the direction of temperature ramping. The first-order ICCDW/NCCDW and NCCDW/CCDW phase transitions are identified as jumps in sample resistance. **b**, Thickness–temperature phase diagram obtained from the measurements in **a**. Blue and black squares mark the ICCDW/NCCDW and NCCDW/CCDW phase boundaries, respectively. For simplicity, only phase boundaries recorded during cooldown are shown. Horizontal error bars represent the uncertainty in sample thickness determination from AFM and optical measurements. Vertical error bars denote the widths of the phase transitions in temperature.

transition was not detected in samples subjected to EDL surface gating under our experimental conditions (Supplementary Section VI), and we attribute this transition to gate-controlled intercalation, which induces high electron doping in individual atomic layers of the thin flake (even though structural modification introduced by Li ion intercalation may also play a role). This is much like the charging process in a Li ion battery where Li ions intercalate into the anode on application of a voltage[31]. Indeed, 1T-TaS_2 crystal has been studied previously for its potential application in batteries[32], and similar gating effects were also observed recently in $NbSe_2$ thin films[33] and graphite[34].

Further investigations support the proposed mechanism of gate-controlled intercalation in our iFET. First, we show that the iFET operates through diffusion—the gate tunability of the sample remains unchanged, even if the sample is only partially in contact with the solid electrolyte. This is demonstrated in Fig. 1d, where the active area of sample B is protected by a layer of 300-nm-thick poly(methyl methacrylate) (PMMA), with only a corner exposed to the solid electrolyte. On gating, sample B (red curve, Fig. 1d) behaved in the same way as sample A (black curve, Fig. 1d), which was entirely exposed. Meanwhile, a fully protected control sample (sample C, blue curve in Fig. 1d) showed no sign of a gating effect. Our finding rules out any alternative mechanisms that require close contact between the sample surface and the electrolyte, and points to diffusion-based intercalation as the most likely scenario.

Second, we show that the 1T-TaS_2 iFET is capable of doping the sample far beyond the critical thickness associated with the electrostatic screening length. A gate voltage applied on the iFET induces an NCCDW/ICCDW phase transition in samples with thicknesses varying from 3.5 nm to 23 nm. Some typical data sets are shown in Fig. 3a (gate bias V_g is swept at 1 mVs^{-1}, and curves are shifted horizontally for clarity). Here, a well-developed ICCDW phase, with a hallmark factor-of-two resistance drop from the initial NCCDW phase, indicates uniform doping in the gate-induced ICCDW phase. Such a uniform ICCDW phase was clearly observed in samples with thicknesses less than 13 nm, but not in thicker samples (Fig. 3a), due to the limited gate-modulation depth. We were able to extract the gate-modulation depth of our iFETs by simplifying the gated sample as two homogeneous slabs (Fig. 3b inset): the uniformly doped upper slab with resistance R_{ICCDW} (low-resistance ICCDW phase) and the undoped lower slab with resistance $R_{NCCDW} = 2R_{ICCDW}$ (high-resistance NCCDW phase). The resulting lowest resistance R_{min}, normalized to the initial resistance R_0 (that is, $r = R_{min}/R_0$), is therefore

$$r = \begin{cases} 0.5 & \text{if } t < t_c \\ 1 - \dfrac{t_c}{2t} & \text{if } t > t_c \end{cases} \quad (1)$$

where t is the sample thickness and t_c is the maximum gate-modulation depth. By fitting our data with the above model, we obtained

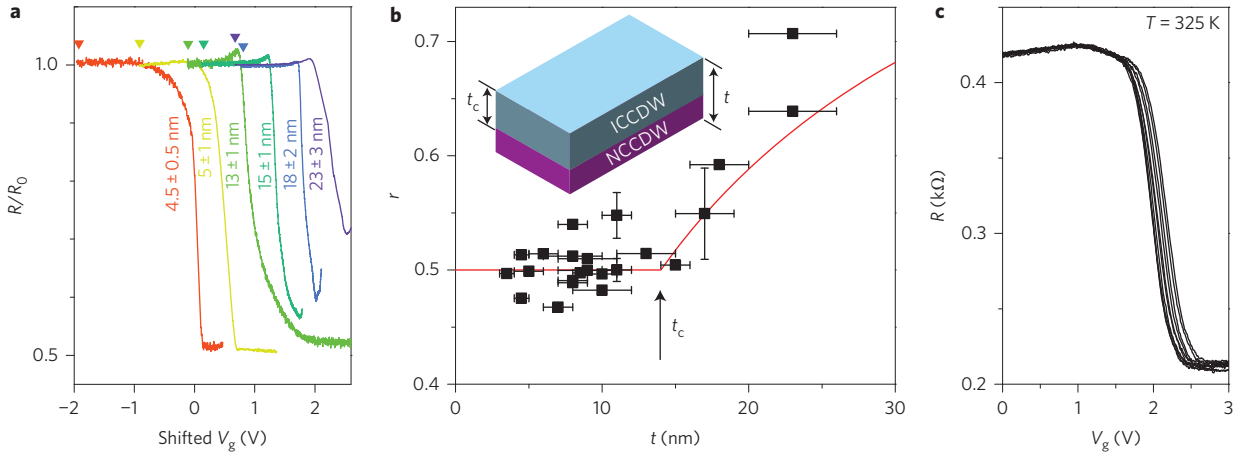

Figure 3 | Gate-modulation depth and repeatability of 1T-TaS_2 iFET. a, Resistance R (normalized to its initial value R_0 in the NCCDW state) shown as a function of V_g for a few typical samples with varying thicknesses. The gate-induced NCCDW/ICCDW phase transition is manifested as the sudden drop in resistance by one-half. Curves are shifted horizontally for clarity, and the origin of each curve is marked by colour-matched triangles. **b**, Ratio r between lowest resistance R_{min} during the gate sweep and initial resistance R_0 in the samples as a function of sample thickness. Red line: Fit according to the model described in the text. Inset: Inhomogeneous doping in the out-of-plane direction assumed in the model, where t_c is the modulation depth of the gate-controlled intercalation (t_c = 14 nm is obtained from the fitting, as indicated by the arrow in the main figure). Horizontal error bars represent the uncertainty in sample thickness determination from AFM and optical measurements. The two vertical error bars are derived from the contact resistance of the two devices measured in a two-terminal geometry. **c**, Resistance of a sample during ten gate sweep cycles (only up-sweeps are shown). No appreciable change is observed after repeated gate sweeps.

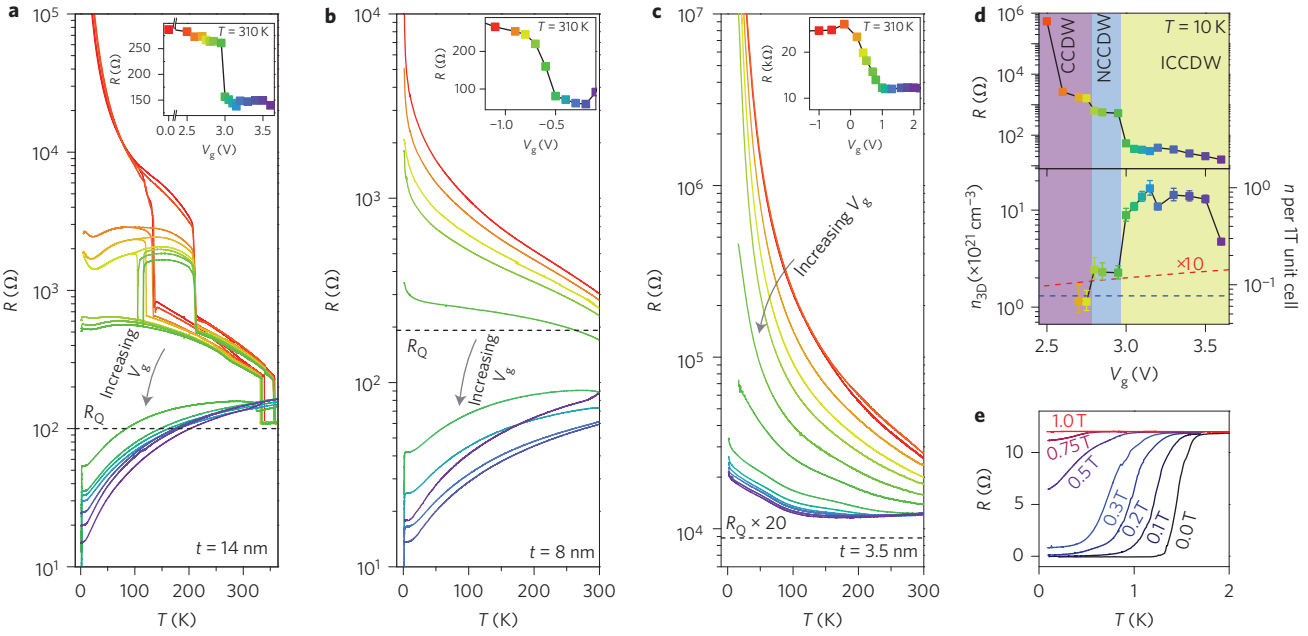

Figure 4 | Electronic transport in 1T-TaS_2 thin flakes under gate-controlled intercalation. a–c, Temperature-dependent resistance at fixed gate voltages for three sample thicknesses: 14 nm, 8 nm and 3.5 nm. The inset in each panel displays the gate-induced NCCDW/ICCDW phase transition at 310 K, which serves as a colour-coded reference of V_g. Arrows in each plot indicate the direction of increasing V_g. Black dashed lines mark the value of R_Q defined in the main text. **d**, Resistance and volumetric carrier density (n_{3D}) measured as a function of V_g at 10 K in the same 14-nm-thick sample shown in **a**. n_{3D} is obtained from the line fit to the Hall resistance, which is much larger than the estimated charge density expected from EDL surface doping[39] (red dashed line; the surface charge density has been converted to volumetric carrier density for easy comparison). Error bars represent the uncertainty of the line fit. Blue dashed line: Doping level corresponding to 1 electron per David-star. **e**, Zero-resistance superconducting state of a typical gated 1T-TaS_2 flake subjected to a varying perpendicular magnetic field.

$t_c \approx 14$ nm (Fig. 3b). We note that even larger critical thicknesses are possible with a slower gate sweep, as the Li ions have more time to diffuse into the sample (Supplementary Section V). Such a gate-modulation depth is much larger than the gating range of EDL, which is limited by the electrostatic screening length (<1 nm), and lends further support to gate-controlled intercalation as the origin of the gate modulation. Finally, we point out that the gate modulation in our iFET is repeatable and reversible (Fig. 3c), suggesting that no chemical modification of the sample occurs during the intercalation cycles. Further investigations of the

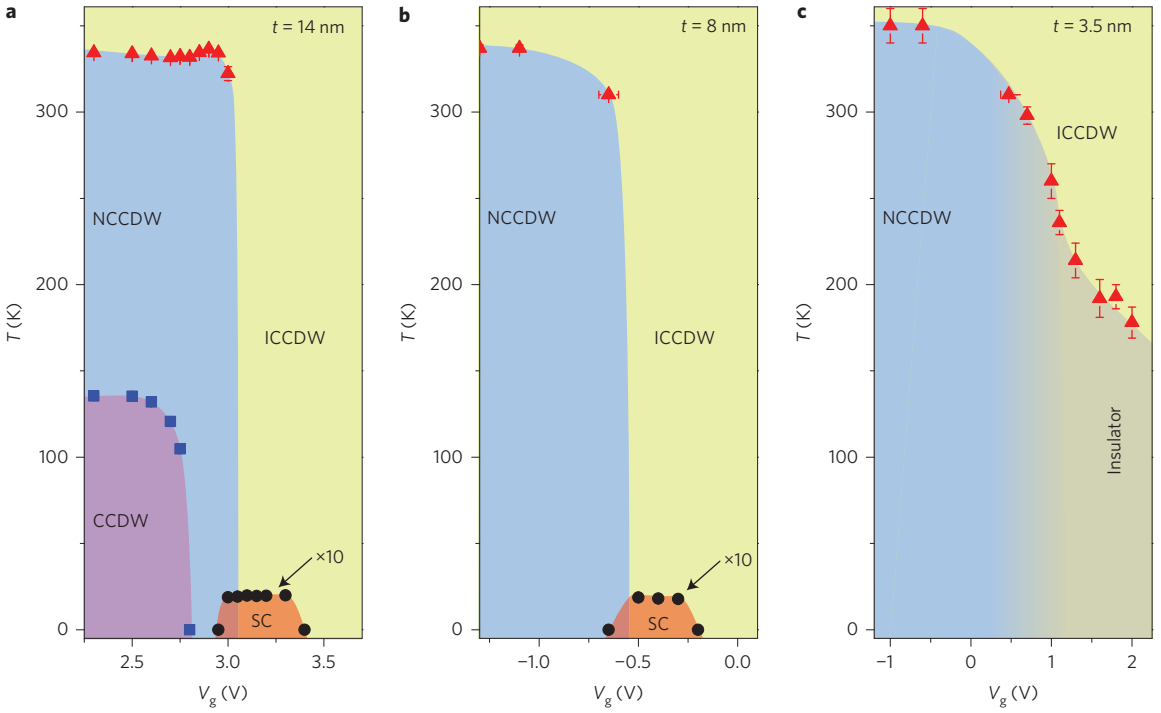

Figure 5 | Doping–temperature phase diagrams of 1T-TaS_2 flakes in three thickness regimes. a–c, Doping–temperature phase diagrams of 1T-TaS_2 thin-flake samples in bulk (**a**), quasi-two-dimensional (**b**) and two-dimensional (**c**) limits, respectively. The diagrams are obtained from the data in Fig. 4a–c. Boundaries of the CCDW, NCCDW and superconducting (SC) phases are marked by blue, red and black symbols, respectively. Only transition temperatures recorded during cooldown are shown for simplicity. The metal–insulator transition temperature in **c** is defined as the temperature where the (initially metallic) sample starts to show insulating behaviour as the temperature is lowered. Horizontal and vertical error bars denote the widths of the phase transitions in V_g and temperature, respectively.

electrochemical intercalation with other ion species are presented in Supplementary Section VI.

Phase transitions tuned by gate-controlled intercalation

The gate-controlled intercalation dramatically modulates the various phase transitions in 1T-TaS_2, which were probed by measuring the temperature-dependent resistance in samples with varying thicknesses. Figure 4 presents the temperature-dependent resistance at various fixed V_g for three sample thicknesses: 14 nm (Fig. 4a), 8 nm (Fig. 4b) and 3.5 nm (Fig. 4c). These three thicknesses were chosen because they represent three distinctive regions in the phase diagram in Fig. 2b: the 14-nm-thick sample retains all the CDW phases found in the bulk, so is within the bulk limit; the 8-nm-thick sample is in the quasi-two-dimensional limit, where all but the CCDW phases remain; finally, in the two-dimensional limit, the 3.5-nm-thick sample is an insulator without obvious phase transitions.

The temperature-dependent resistance of the 14-nm-thick sample is shown in Fig. 4a. For clarity, the gate-induced NCCDW/ICCDW phase transition at room temperature is used as a map (shown in the inset), where the V_g is colour-coded to match the values used in each temperature sweep. On gating, the resistance was strongly suppressed in the entire CCDW phase starting from $V_g = 2.6$ V, even though all phase transition temperatures remained unaffected (Fig. 4a, orange curve). We attribute the observed resistance suppression to gate-induced melting of the Mott state inside the CCDW phase. The fact that the CCDW phase survives the Mott phase indicates that the Mott localization is not the driving force but rather a consequence of the CCDW transition, in contrast to the findings of recent studies[35–38]. An increasing V_g depressed the NCCDW/CCDW transition temperature and eventually eliminated the transition altogether. The sample then became metallic, with room-temperature resistivity per layer on the order of the quantum resistance R_Q, defined as $h/4e^2$ (as a reference, the expected sample resistance corresponding to R_Q is shown as a dashed line in Fig. 4a), where h is Plank's constant and e is the elementary charge. A superconducting phase emerges inside the NCCDW phase, and is characterized by a well-defined zero-resistance state below $T_c = 2$ K and an upper critical field of $H_{c2} \approx 0.7$ T (Fig. 4e and Supplementary Section VIII). Further increasing the gate doping eliminated the ICCDW/NCCDW transition, while the superconductivity persisted to high doping levels with no appreciable change in T_c, before disappearing into a metallic state at $V_g \geq 3.3$ V. Figure 5a summarizes our observations in a doping–temperature phase diagram. We note that the sharp transitions between various phases indicate a mostly homogeneous sample (see Supplementary Section V for a detailed discussion). However, doping inhomogeneity (such as filamentary paths) cannot be entirely ruled out. Such inhomogeneity may conspire with the phase separation intrinsic to the first-order transitions and produce the observed behaviours in our devices.

The dramatic effect of gate doping is most visible at low temperatures, where the normal state resistance spans five orders of magnitude under gating (Fig. 4d, upper panel). Three regions corresponding to CCDW, NCCDW and ICCDW phases are readily identified and we determined the volumetric charge carrier density n_{3D} in the three phases from Hall measurements at $T = 10$ K (Fig. 4d, lower panel). As soon as the Mott phase was suppressed at $V_g = 2.6$ V, the CCDW state gained a carrier density that corresponds to ~1e per David-star (blue dashed line in Fig. 4d), as expected from a melted Mott state. Further doping significantly increased the carrier density and eventually reached ~1e per Ta atom. Such an extremely high carrier concentration is almost two orders of magnitude higher than the maximum doping expected from EDL gating[39] (red dashed line,

Fig. 4d) and further corroborates our proposed mechanism of gate-controlled intercalation.

It is important to note that only part of the charge density measured here originates from charges transferred from intercalated Li. Our first-principle calculations show that each Li atom donates ~0.2 electrons, on average, to the host, and the maximum intercalation density is estimated to be one Li atom per Ta (Supplementary Section IX). Accordingly, charge transfer can only account for ~20% of the maximum observed charge density at most. The rest most probably comes from structural/electronic modifications induced by intercalation and associated phase transitions. Indeed, the doping-dependent resistance (Fig. 4d) and phase diagram (Fig. 5a) of our gated 1T-TaS_2 are strikingly similar to those reported in ref. 14, if one replaces doping with pressure. Such a similarity may indicate a deep connection between the two, as Li ions possibly introduce structural modifications (that is, an effective 'pressure') as well as charge doping. Future diffraction/microscopy experiments are needed to delineate the exact role of Li intercalation. Finally, we note that the absolute V_g value does not directly quantify the extent of gate doping because of the large hysteresis observed during gate sweeps (Supplementary Section V). However, the gating behaviour is robust in all our iFETs tested (41 devices in total), even though V_g at the phase transitions varies from sample to sample. We instead use the carrier concentration obtained from Hall measurements as a quantitative measure of the doping level (Fig. 4d).

The gate-controlled intercalation also has a marked effect on the 8-nm-thick sample. In this case the CCDW phase (and the associated Mott phase) was absent due to the reduced dimensionality, but the remaining phases evolved in a pattern similar to that in the 14-nm-thick sample (Fig. 4b, ICCDW/NCCDW transition not shown). Meanwhile, the 3.5-nm-thick sample remained insulating at low temperatures ($T < 100$ K), probably due to disorders, and gating only partially suppressed the insulating phase (Fig. 4c). These observations are summarized in the phase diagrams in Fig. 5b,c.

The new phase diagrams for 1T-TaS_2 provide fresh insights into the intricate relation between various charge-ordered phases and superconductivity (Fig. 5). An important clue lies in the doping–temperature phase diagram in the quasi-two-dimensional limit (Fig. 5b). Here, the CCDW phase collapses due to reduced dimensionality, but all other phases, including the superconducting phase, remain intact. This observation leads us to conclude that the CCDW phase (and therefore the Mott phase inside it) is not directly responsible for the superconductivity. The question then arises as to what causes the superconductivity in 1T-TaS_2. To this end, we point out that the superconductivity appears at the intersection of NCCDW and ICCDW, where mesoscopic/microscopic phase separation is likely to occur due to the first-order nature of the transition[40,41]. Because the system is not superconducting deep in either phase, we speculate that the microscopically separated ICCDW/NCCDW phase at the intersection may cooperate to provide the right amount of electron–phonon interaction for Cooper pairing.

Conclusion

We have developed a new device, referred to as an iFET, and used it to controllably intercalate Li ions into the atomic layers of 1T-TaS_2 with an externally applied gate voltage. Tremendous charge doping is achieved, and we are able to modulate the electronic properties of the 1T-TaS_2 through gate-induced phase transitions. The findings shed new light onto the intricate interplay of various phases in 1T-TaS_2 thin flakes. Our *in situ* gate-controlled intercalation, as a general method for continuous, reversible tuning of material properties of two-dimensional atomic crystals, opens up new opportunities in searching for novel materials and devices in the extreme doping limit.

Note added in proof: We have become aware of related work on 1T-TaS_2 (ref. 42).

Methods

Device fabrication. High-quality 1T-TaS_2 single crystals were grown using a standard chemical vapour transport method. 1T-TaS_2 thin flakes were obtained by mechanically exfoliating bulk single crystals onto an Si wafer covered with a 285-nm-thick thermally grown SiO_2 layer (a quartz substrate was also used in some of our devices, and no difference was observed in terms of device characteristics). Optical microscopy and atomic force microscopy (AFM, Park Systems XE-120) were used to characterize the quality and thickness of the thin flakes. Once thin flakes were identified on the substrate, metal electrodes (Au, typical thickness ~40 nm) were deposited using either a standard electron-beam lithography process or direct evaporation through a stencil mask. Sample degradation was observed in thin flakes stored in air (see Supplementary Section II for details), so air exposure was minimized during the fabrication process to mitigate the degradation of the sample.

$LiClO_4$ (Sigma Aldrich) dissolved in PEO (M_w = 100,000, Sigma Aldrich) matrix was used as the solid electrolyte[39,43]. $LiClO_4$ and PEO powders (0.3 g and 1 g, respectively) were mixed with 15 ml anhydrous methanol (Alfa Aesar). The mixture was then stirred overnight with the temperature kept at 50 °C. Note that the ratio between $LiClO_4$ and PEO is crucial for the performance of the electrolyte. After application of the electrolyte, all samples were annealed at 370 K in vacuum (~30 Pa) for half an hour to eliminate residual methanol and moisture before the gate sweep.

Measurements. Transport measurements were mainly performed in an Oxford Instruments Integra AC cryostat. The sample resistance was measured using a lock-in amplifier (Stanford Research 830), and the gate voltage was supplied by a Keithley 2400 source meter. V_g was swept at fixed temperatures between 310 K and 370 K in vacuum. Before each cooldown, the temperature and gate voltage were held constant for half an hour to ensure samples were homogeneously intercalated.

Received 13 July 2014; accepted 10 December 2014; published online 26 January 2015

References

1. Imada, M., Fujimori, A. & Tokura, Y. Metal–insulator transitions. *Rev. Mod. Phys.* **70,** 1039 (1998).
2. Ahn, C. H., Triscone, J-M. & Mannhart, J. Electric field effect in correlated oxide systems. *Nature* **424,** 1015–1018 (2003).
3. Ahn, C. H. *et al.* Electrostatic modification of novel materials. *Rev. Mod. Phys.* **78,** 1185–1212 (2006).
4. Glover, R. E. & Sherrill, M. D. Changes in superconducting critical temperature produced by electrostatic charging. *Phys. Rev. Lett.* **5,** 248–250 (1960).
5. Mannhart, J., Bednorz, J. G., Müller, K. A. & Schlom, D. G. Electric field effect on superconducting $YBa_2Cu_3O_{7-\delta}$ films. *Z. Für Phys. B Condens. Matter* **83,** 307–311 (1991).
6. Ahn, C. H. *et al.* Electrostatic modulation of superconductivity in ultrathin $GdBa_2Cu_3O_{7-x}$ films. *Science* **284,** 1152–1155 (1999).
7. Parendo, K. A. *et al.* Electrostatic tuning of the superconductor–insulator transition in two dimensions. *Phys. Rev. Lett.* **94,** 197004 (2005).
8. Fazekas, P. & Tosatti, E. Electrical, structural and magnetic properties of pure and doped 1T-TaS_2. *Phil. Mag. B* **39,** 229–244 (1979).
9. Kim, J-J., Yamaguchi, W., Hasegawa, T. & Kitazawa, K. Observation of Mott localization gap using low temperature scanning tunneling spectroscopy in commensurate 1T-TaS_2. *Phys. Rev. Lett.* **73,** 2103–2106 (1994).
10. Zwick, F. *et al.* Spectral consequences of broken phase coherence in 1T-TaS_2. *Phys. Rev. Lett.* **81,** 1058–1061 (1998).
11. Wilson, J. A., Di Salvo, F. J. & Mahajan, S. Charge-density waves and superlattices in the metallic layered transition metal dichalcogenides. *Adv. Phys.* **24,** 117–201 (1975).
12. Scruby, C. B., Williams, P. M. & Parry, G. S. The role of charge density waves in structural transformations of 1T TaS_2. *Philos. Mag.* **31,** 255–274 (1975).
13. Thomson, R. E., Burk, B., Zettl, A. & Clarke, J. Scanning tunneling microscopy of the charge-density-wave structure in 1T-TaS_2. *Phys. Rev. B* **49,** 16899–16916 (1994).
14. Sipos, B. *et al.* From Mott state to superconductivity in 1T-TaS_2. *Nature Mater.* **7,** 960–965 (2008).
15. Ritschel, T. *et al.* Pressure dependence of the charge density wave in 1T-TaS_2 and its relation to superconductivity. *Phys. Rev. B* **87,** 125135 (2013).
16. Ang, R. *et al.* Real-space coexistence of the melted Mott state and superconductivity in Fe-substituted 1T-TaS_2. *Phys. Rev. Lett.* **109,** 176403 (2012).
17. Ang, R. *et al.* Superconductivity and bandwidth-controlled Mott metal–insulator transition in 1T-$TaS_{2-x}Se_x$. *Phys. Rev. B* **88,** 115145 (2013).
18. Misra, R., McCarthy, M. & Hebard, A. F. Electric field gating with ionic liquids. *Appl. Phys. Lett.* **90,** 052905 (2007).
19. Ueno, K. *et al.* Electric-field-induced superconductivity in an insulator. *Nature Mater.* **7,** 855–858 (2008).

20. Ye, J. T. *et al.* Liquid-gated interface superconductivity on an atomically flat film. *Nature Mater.* **9,** 125–128 (2010).
21. Pillo, T. *et al.* Remnant Fermi surface in the presence of an underlying instability in layered 1T–TaS_2. *Phys. Rev. Lett.* **83,** 3494–3497 (1999).
22. Spijkerman, A., de Boer, J. L., Meetsma, A., Wiegers, G. A. & van Smaalen, S. X-ray crystal-structure refinement of the nearly commensurate phase of 1T-TaS_2 in (3+2)-dimensional superspace. *Phys. Rev. B* **56,** 13757–13767 (1997).
23. Tidman, J. P. & Frindt, R. F. Resistivity of thin TaS_2 crystals. *Can. J. Phys.* **54,** 2306–2309 (1976).
24. Williams, P. M., Scruby, C. B., Clark, W. B. & Parry, G. S. Charge density waves in the layered transition metal dichalcogenides. *J. Phys. Colloq.* **37,** C4-139–C4-150 (1976).
25. Moncton, D. E., DiSalvo, F. J., Axe, J. D., Sham, L. J. & Patton, B. R. Charge-density wave stacking order in 1T-$Ta_{1-x}Zr_xSe_2$: interlayer interactions and impurity (Zr) effects. *Phys. Rev. B* **14,** 3432–3437 (1976).
26. Bulaevskii, L. N. & Khomskii, D. I. Three-dimensional ordering of charge-density waves in quasi-one-dimensional and layered crystals. *J. Exp. Theor. Phys.* **46,** 608–615 (1977).
27. Walker, M. B. & Withers, R. L. Stacking of charge-density waves in 1T transition-metal dichalcogenides. *Phys. Rev. B* **28,** 2766–2774 (1983).
28. Bovet, M. *et al.* Interplane coupling in the quasi-two-dimensional 1T-TaS_2. *Phys. Rev. B* **67,** 125105 (2003).
29. Nakanishi, K. & Shiba, H. Theory of three-dimensional orderings of charge-density waves in 1T-TaX_2 (X: S, Se). *J. Phys. Soc. Jpn* **53,** 1103–1113 (1984).
30. Tanda, S., Sambongi, T., Tani, T. & Tanaka, S. X-ray study of charge density wave structure in 1T-TaS_2. *J. Phys. Soc. Jpn* **53,** 476–479 (1984).
31. Whittingham, M. S. Lithium batteries and cathode materials. *Chem. Rev.* **104,** 4271–4302 (2004).
32. Thompson, A. H. Electrochemical studies of lithium intercalation in titanium and tantalum dichalcogenides. *Physica B+C* **99,** 100–106 (1980).
33. Li, Z. J., Gao, B. F., Zhao, J. L., Xie, X. M. & Jiang, M. H. Effect of electrolyte gating on the superconducting properties of thin 2H-$NbSe_2$ platelets. *Supercond. Sci. Technol.* **27,** 015004 (2014).
34. Bao, W. *et al.* Approaching the limits of transparency and conductivity in graphitic materials through lithium intercalation. *Nature Commun.* **5,** 4224 (2014).
35. Perfetti, L. *et al.* Time evolution of the electronic structure of 1T-TaS_2 through the insulator–metal transition. *Phys. Rev. Lett.* **97,** 067402 (2006).
36. Hellmann, S. *et al.* Ultrafast melting of a charge-density wave in the Mott insulator 1T-TaS_2. *Phys. Rev. Lett.* **105,** 187401 (2010).
37. Eichberger, M. *et al.* Snapshots of cooperative atomic motions in the optical suppression of charge density waves. *Nature* **468,** 799–802 (2010).
38. Petersen, J. C. *et al.* Clocking the melting transition of charge and lattice order in 1T-TaS_2 with ultrafast extreme-ultraviolet angle-resolved photoemission spectroscopy. *Phys. Rev. Lett.* **107,** 177402 (2011).
39. Efetov, D. K. & Kim, P. Controlling electron–phonon interactions in graphene at ultrahigh carrier densities. *Phys. Rev. Lett.* **105,** 256805 (2010).
40. Dagotto, E. Complexity in strongly correlated electronic systems. *Science* **309,** 257–262 (2005).
41. Joe, Y. I. *et al.* Emergence of charge density wave domain walls above the superconducting dome in 1T-$TiSe_2$. *Nature Phys.* **10,** 421–425 (2014).
42. Yoshida, M. *et al.* Controlling charge-density-wave states in nano-thick crystals of 1T-TaS_2. *Sci. Rep.* **4,** 7302 (2014).
43. Fullerton-Shirey, S. K. & Maranas, J. K. Effect of $LiClO_4$ on the structure and mobility of PEO-based solid polymer electrolytes. *Macromolecules* **42,** 2142–2156 (2009).

Acknowledgements

The authors thank D-H. Lee for critical reading of the manuscript, Z-X. Shen, P. Kim, F. Wang, L. Zhou, J. Zhao, Y. Wang, W. Wu, P. Darancet and J. Liu for helpful discussions, and X. Hong, L. He, K. Yu and L. Sun for assistance with measurements. Part of the sample fabrication was conducted at Fudan Nano-fabrication Laboratory. Y.Y., F.Y., L.M. and Y.Z. acknowledge financial support from the National Basic Research Program of China (973 Program) under grants nos. 2011CB921802 and 2013CB921902, and from the NSF of China under grant no. 11034001. X.F.L., Y.J.Y. and X.H.C. are supported by the 'Strategic Priority Research Program (B)' of the Chinese Academy of Sciences (grant no. XDB04040100) and the NSF of China (grant no. 11190021). Y-W.S. is supported by the NRF of Korea grant funded by MEST (QMMRC, no. R11-2008-053-01002-0). The work at Rutgers is funded by the Gordon and Betty Moore Foundation's EPiQS Initiative through Grant GBMF4413 to the Rutgers Center for Emergent Materials, and the work at Postech is supported by the Max Planck POSTECH/KOREA Research Initiative Program (grant no. 2011-0031558) through the NRF of Korea funded by MEST.

Author contributions

Y.Z. conceived the project. X.F.L., Y.J.Y., Y.H.C., S.W.C. and X.H.C. grew bulk 1T-TaS_2 crystal. Y.Y. fabricated 1T-TaS_2 thin-film devices, performed electric measurements and analysed the data. F.Y. made the solid electrolyte. L.M. carried out scanning tunnelling microscopy measurement on 1T-TaS_2 thin films. Y.Y. and Y.Z. analysed the data. X.N. and D.F. performed angle-resolved photoemission spectroscopy measurement on bulk 1T-TaS_2 crystal. S.K. and Y.W.S. carried out *ab initio* calculations. S.L. helped with low-temperature measurements. Y.Y. and Y.Z. wrote the paper and all authors commented on it.

Additional information

Supplementary information is available in the online version of the paper. Reprints and permissions information is available online at www.nature.com/reprints. Correspondence and requests for materials should be addressed to Y.Z.

Competing financial interests

The authors declare no competing financial interests.